Enhancing Metabolite Coverage in MALDI-MSI using Laser Post-Ionisation (MALDI-2).

J.C.McKinnon,[a] H.H.Milioli,[c,d,e] C.Purcell,[c,d,e] C.Chaffer,[c,d,e] B.Wadie,[f] T.Alexandrov,[f] T.W.Mitchell[b] and S.R.Ellis[*a]

[a] Molecular Horizons and School of Chemistry and Molecular Bioscience, University of Wollongong, Northfields Ave, Wollongong, NSW 2522, Australia.

[b] Molecular Horizons and School of Medical, Indigenous and Health Science, University of Wollongong, Northfields Ave, Wollongong, NSW 2522, Australia

[c] Garvan Institute of Medical Research, Darlinghurst, NSW, Australia

[d] St. Vincent's Clinical School, UNSW Medicine, UNSW Sydney, NSW, Australia

[f] The Kinghorn Cancer Centre, Darlinghurst, NSW, Australia

[g] Structural and Computational Biology Unit, European Molecular Biology Laboratory (EMBL), Heidelberg, Germany.

[*] To whom correspondence should be addressed

Email: sellis@uow.edu.au

Abstract

Matrix-assisted laser desorption/ionisation mass spectrometry imaging (MALDI-MSI) of metabolites can reveal how metabolism is altered throughout heterogeneous tissues. Here MALDI-MSI has been coupled with laser post-ionsiation (MALDI-2) and applied to the MSI of metabolites for the first time. Using mouse kidney and tumour-bearing liver tissue, MALDI-2 significantly improved metabolite coverage and the detection sensitivity of many metabolites. This approach provides a significant advancement for metabolite MSI, enabling the metabolic environment of tissues to be imaged at increased levels of detail.

Introduction

Matrix-assisted laser desorption/ionisation mass spectrometry imaging (MALDI-MSI) is a maturing technology enabling multiplexed and label-free imaging of many analyte classes, including metabolites[1], pharmaceuticals[2], lipids[3], glycans[4], and proteins[5] directly from thin tissue sections, single cells[6,7], and other substrates such as large polymer biomaterials[8,9]. Recently, the application of MALDI-MSI to imaging small metabolites[10] has received increasing interest. MSI of metabolites can provide unqiue insight into the metabolic alterations caused by many diseases and metabolic perturbations[11,12] such as ischemic stroke[13], migraine[14], kidney repair[15] as well as metabolism in non-mammlian samples such as plants.[16] Metabolite imaging using MSI is also a very promising appoach for mapping metabolic changes within tumours where the metabolic environment is significantly altered, for example, by the Warburg effect. Examples of MALDI-MSI of metabolite distributions in cancer include glioblastoma[17], thyroid cancer subtypes[18], pancreatic ductul adenocarcinoma[19] and breast cancer brain metastasis.[20]

MALDI-MSI of metabolites is typically performed in the negative-ion mode using matrices 9-aminoacridine (9-AA), diaminonaphthalene (DAN) and N-(1-naphthyl) ethylenediamine dihydrochloride (NEDC).[21] However, analyte coverage is often limited by varied and often low ionisation efficiencies of analytes (as low as 10-9), an effect further compounded by the complex nature of biological samples leading to ion suppression effects. To help overcome this limitation and broaden the overall analyte coverage and sensitivity of MSI, post-ionisation (PI) techniques that enhance ionisation efficiencies by up to 2-orders of magnitude have seen rapid development in recent years. These PI methods add an additional ionisation event that helps ionise analytes not ionised by the initial ionisation event (e.g., MALDI). A variety of PI methods have been reported including those reliant on the interaction of neutral analytes with reactive species generated by a cold plasma[22], dopants ionised by VUV

photons[23] and laser-post-ionisation (MALDI-2)[24]. MALDI-2 is the most widely adopted PI method. It involves the irradiation of the MALDI plume 10-20 µs after generation by the MALDI laser with a second laser pulse below the two-photon threshold of the matrix (often <280 nm). When performed under elevated pressure conditions to maintain plume density (3-10 mbar), this induces a second MALDI-like ionisation event spatially and temporally separated from the MALDI process. MALDI-2 has shown significant benefits for lipids[25,26], pharmaceuticals[27], N-glycans[28] and tryptic peptides[29]. For example, applied to liver tissue at 20 µm pixel size, MALDI-2 was capable of detecting ~7-times more lipid species than conventional MALDI in positive-ion mode[30]. The sensitivity gain offered by MALDI-2 has also facilitated spatial resolution improvement in MALDI-MSI of lipids to 1 µm[31]. However, the benefits of MALDI-2 for imaging low molecular weight metabolites have not been investigated. Herein, we have investigated MALDI-2 for metabolite imaging of kidney and tumour tissue and show it allows detection and imaging of a broader range of metabolites than conventional MALDI.

Experimental Methods

Materials

Methanol (MeOH), N-(1-naphthyl) ethylenediamine dihydrochloride (NEDC) matrix and water (LC-MS grade) were purchased from Merck (Darmstadt, Germany). Haematoxylin and eosin were purchased from POCD Scientific (North Rocks NSW, Australia).

Biological samples

Homogenates used for optimisation experiments were prepared from fresh bovine liver sourced from a local butcher. Briefly, 100 g of tissue was homogenised via a food processor with 20 mL of 2% carboxymethylcellulose in water and flash-frozen in liquid nitrogen prior to storage at -80 °C. Kidney of a wild-type mouse (5 month old male) was provided in accordance with the Australian code for care and use as residual tissue from prior animal studies conducted at the university. Following euthanasia via isoflurane, organs including the kidney were collected immediately and were flash-frozen in liquid nitrogen prio to storage at -80 °C.

Breast cancer metastases in the liver where obtained by inoculating the triple-negative breast cancer cell line (MDA-MB-231) cell line into the mammary fatpad. Animals were monitored weekly and sacrificed when primary tumours reached ethical endpoint (1000mm^3; ~12 weeks). Liver tissue containing spontaneous metastases was collected, sectioned, embedded in OCT media and transferred to storage at -80°C. Experiments were approved by and conducted in accordance with the National Health and Medical Research Council Statement on Animal Experimentation, the requirements of New South Wales State Government legislation, and with the rules for animal experimentation of the Biological Testing Facility of the Garvan Institute and the Victor Chang Cardiac Research Institute (protocol #18/12).

Sample preparation

Liver homogenates, mouse kidney and the tumour bearing liver tissues were sectioned at 10-15 µm thickness using a cryo-microtome (Leica, Nussloch GmbH, Germany) at -20°C and thaw-mounted onto microscope glass slides. Following sectioning, samples were stored at -80°C until required. Once required, all tissue sections were coated with NEDC matrix using an automatic sprayer (TM-Sprayer, HTX Technologies, LLC, Chapel Hill, NC, USA). NEDC matrix was dissolved in a 7:3 mixture of MeOH:Water (v:v) at a concentration of 14 mg/mL.

18 layers of matrix solution was deposited using a flow rate of 0.05 mL/min, 10 psi of N_2 pressure, nozzle temperature of 80°C and a 1200 mm/min velocity. Matrix density is reported at 0.003500 mg/mm^2.

Tissue staining

Both the kidney and tumour-bearing liver tissue sections were stained with hematoxylin and eosin (H&E) for post-MSI histological analysis via light microscopy. The H&E protocol was as follows: the glass slides were immersed in 95% ethanol, 70% ethanol and H_2O for 2 minutes each and then immersed in haematoxylin for 3 minutes. Slides were then washed with running tap water for 3 minutes and immersed in eosin for 30 seconds following immersion in 100% ethanol for 1 minute and xylene for 30 seconds.

Microscopy

Light microscopy using a SP8 Falcon confocal microscope (Leica Microsystems, Germany) with a 10x objective was used for optical imaging of stained tissues.

Mass spectrometry instrumentation

All data were acquired using an Orbitrap Elite mass spectrometer (Thermo Fisher Scientific GmbH, Bremen, Germany) coupled to an intermediate pressure MALDI source (Spectroglyph LLC, WA, USA) as described previously[1]. Unless specified otherwise, the HPF was operated at an amplitude of ~100 V_{P-P} and frequency of 570 kHz, and the LPF operated at an amplitude of ~44 V_{P-P} and frequency of 840 kHz. Except for pressure optimisation experimtns the HPF pressure was controlled to be 4 Torr with the convectron gauge of the Orbitrap Elite maintained at 1.5 Torr.

A frequency tripled Nd:YLF laser (Explorer One, Spectra Physics, Mountain View, CA) emitting at 349 nm operating at 300 Hz was used for desorption and MALDI (referred to throughout as the MALDI laser). The MALDI laser was operated at a diode current of 1.8 A, with the pulse energy fine-tuned with an external attenuator (PowerXP, Altechna, Vilnius, Lithuania) positioned immediately in front of the laser. A pulse energy of 1.44 µj was used for laser desorption.

For laser post-ionisation (MALDI-2), a frequency quadrupled Nd:YAG laser emitting at 266 nm and operated at a frequency of 300 Hz was used (Nano L-DPSS, Litron Lasers, UK). The MALDI-2 beam was guided into the MALDI ion source to be parallel with the sample surface at an approximate height of 400 µm using a series of mirrors (NB1-K04, Thor Labs, New Jersey, USA) and then focussed via a single plano-convex lens (f = 500 mm, LA4184-U, Thor Labs, New Jersey, USA). Laser pulse energy was controlled using the internal attenuator and adjusted to be 600 µJ as measured using a calibrated energy sensor (QE12HR-H-MB-D0, Gentec-EO, Quebec, Canada) just before the beam entered the ion source. The Explorer MALDI laser provides a triggering signal recorded with an internal photodiode that can be used for synchronisation with the MALDI-2 laser, while an external photodiode was used to monitor the timing of the MALDI-2 laser. To precisely control the timing (i.e., the delay between the laser pulses), both lasers were externally triggered using a Quantum pulse generator (QC9200, Quantum Composers, Bozeman, Montana) such that the time delay between the MALDI and MALDI-2 laser pulse was 6 µs. Pulse delay was determined by monitoring the photodiode outputs using a digital oscilloscope (RIGOL, Portland, USA). A schematic of the post-ionisation setup is included in Fig.S1.

In order to enhance the detection of metabolites using the MALDI-2-MSI method, several essential parameters, such as MALDI laser energy, MALDI-2 laser energy, post-ionisation delay time, RF voltages, and ion source pressure, were assessed on liver homogenate tissue. The optimisation experiments were carried out by performing n=3 line scans across the tissue section while varying one parameter at a time during the MALDI stage flyback. Consequently, each new line scan began with a modified parameter value, allowing for a an evaluation of the impact of each parameter on metabolite detection..

MSI Data Acquisitions

All MSI data was acquired in the negative polarity using a 120,000 FWHM (at *m/z* 400) mass resolving power and a 250 ms injection time. This resulted in a scan time of ~ 1.46 scan/sec Adjacent or nearby tissue sections were imaged using conventional MALDI to compare the effects of post-ionisation on metabolite imaging. All data was acquired using an *m/z* range of 100-1000 and externally recalibrated using the Xcalibur version 3.0.63 Recal Offline Software (Thermo Fisher Scientific) using the known masses of NEDC clusters (*m/z* 257.0618, 479.1542

and 701.2465). For MALDI-MSI and MALDI-2-MSI of mouse kidney sections, a pixel size of 60 µm x 60 µm was used. For the cancerous tissue a pixel size of 20 µm x 20 µm was used.

Data visualisation

Raw data files were first converted from the .raw format into mzml format using version 3.0.2 of the command-line utility msConvertGUI, commercially available from the open-source platform ProteoWizard[2]. The mzml file and the associated position file (xml format) were then combined to produce the MSI data in the vendor neutral imzml format (profile mode) using the in-built converter of Lipostar MSI (Molecular Horizon srl, Bettona, Italy)[3,4]. The resulting imzml file was then loaded into Lipostar MSI for all subsequent data analysis and visualisation.

Datasets were imported with the following Lipostar parameters: 5 ppm *m/z* tolerance, peak intensity > 1% base peak intensity, peak detection frequency > 1% and a minimum spatial chaos > 0.7. Ion images were displayed as TIC normalised and visualised with the viridis colour settings (except when ion images are overlayed) with hotspot removal (high quantile of 99%) and no linear interpolation or denoising applied.

Co-localisation Analysis

In order to identify and compare the number of tumour-specific or enriched metabolites that could be detected with MALDI-2 as opposed to conventional MALDI, a co-localisation analysis was applied. Briefly, the tumour-bearing area of the liver metastasis was defined and guided via histology to determine the region-of-interest (ROI) and co-registration of the MSI data using LipostarMSI. From here, a list of *m/z* values having Pearson correlation coefficients with the tumour ROI ≥0.6 were extracted.

Determination of Number of Tissue-Specific m/z values.

Custom scripts written in the Python programming language were used to determine the number of tissue-specific peaks using the pymsfilereader, NumPy and pandas libraries. First, the averaged mass spectrum from each tissue section and a region only containing matrix were generated and peaks with signal-to-noise values above 5 (for tissue spectrum) and above 3 (for matrix only spectrum) picked. Peaks present in both datasets within a tolerance of 3 ppm were then assumed to arise from the matrix and not the tissue.

Comparison With Existing METASPACE Datasets

To upload data to METASPACE centroid mode imzML files were first created using Image Insight Software (Spectroglyph LLC, Kennewick, WA, USA) using a peak intensity threshold of 5. The resulting imzML files were uploaded to METASPACE for further analysis. To compare against similar datasets in METASPACE, the annotation results for all kidney datasets where the matrix is NEDC and organism is either Human or Mouse were downloaded using the METASPACE API[5] for a total of 140 datasets. In all datasets, only on-sample annotations at FDR 10% against HMDB, CoreMetabolome and SwissLipids were considered. In addition, the following two constraints were applied : (1) only annotations detected in at least 2 MALDI-2 datasets were considered, and (2) only annotations detected in at least 10% (14/140) METASPACE datasets were considered for comparison.

Results and Discussion

First, we optimised ion source parameters for the detection of low molecular weight (LMW) metabolites. We observed that reducing the high-pressure funnel RF amplitudes and reducing the ion source pressure from the conventional setting of 7.5 Torr to 4 Torr increased ion signals observed between m/z 100-1000 (Fig.S2, ESI†). Next, we optimised the time delay between the MALDI and PI laser pulses. The optimal delay time depends on the distance of the PI laser above the sample surface and the velocity of the MALDI plume. The optimal delay time was found to be 6 µs (Fig.S3, ESI†) for the detection of low mass (<m/z 400) metabolites. These optimised parameters were used for all subsequent experiments.

Next, we investigated the metabolite coverage obtained using conventional MALDI and MALDI-2 using mouse kidney tissue (n=3 for MALDI and MALDI-2) at a pixel size of 60 µm. Fig.1a shows the averaged MALDI (black) and MALDI-2 (red) spectra from one kidney section following the removal of background peaks (see ESI† for details). MALDI-2 increased both signal intensity, e.g. the base peak at m/z 124.0078 assigned to the [M-H]$^-$ of taurine increased 4-fold (Fig. 1a) and the number of tissue-related signals. Fig.1b compares the number of tissue-related signals observed across the n=3 tissues for MALDI and MALDI-2 (details provided in ESI†). This data demonstrates that MALDI-2 enables the detection of almost double the number of tissue-related signals compared to conventional MALDI. Fig.1c-g show selected metabolite signals and spatial distributions that are enhanced with MALDI-2 and cover a variety of metabolic classes. Identifications are based on accurate mass (<3 ppm error), matched to the Human Metabolome Database and Metabolomics Workbench, although the presence of isomers cannot be discounted. Fig.1c shows the MALDI-2 distributions of the [M-H]$^-$ ion of the amino acid arginine, which is localised relatively homogenously throughout the kidney. Fig.1d shows the distribution of hexose representing many possible $C_6H_{12}O_6$ isomers localised to the medulla. The detection of [hexose-H]$^-$ also offers enhanced structure

elucidation capabilities upon MS/MS due to resulting cross-ring cleavages. By contrast, hexose is only detected as the [M+Cl]$^-$ ion with conventional MALDI using NEDC, which yields limited structural information upon MS/MS.[6] Fig.1e-g shows the distributions of the [M-H]$^-$ ions of 3-phosphoglyceric acid, uridine and inosine each localised primarily to the cortex.
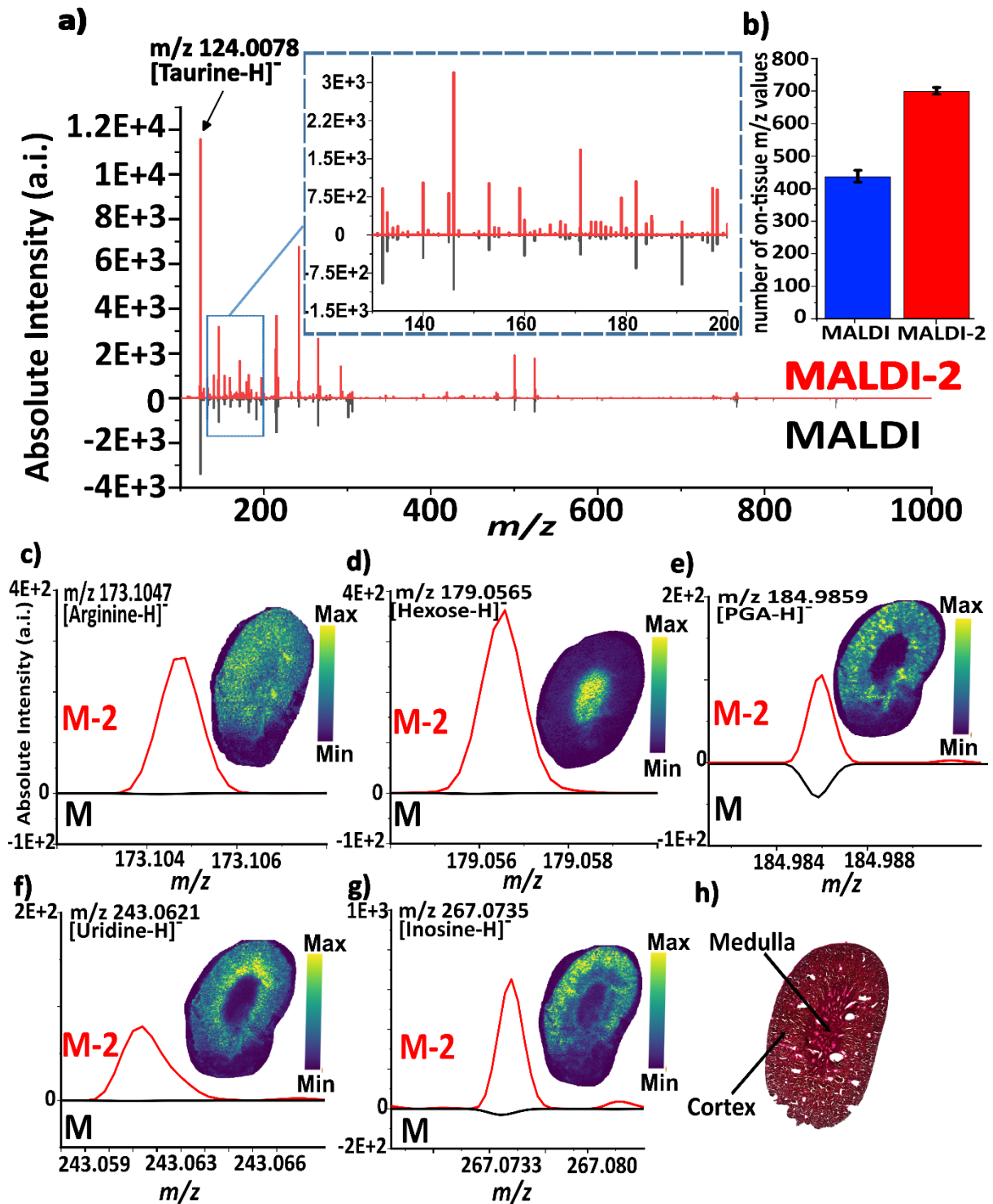
Figure 1: (a) Averaged background subtracted spectra from MALDI (black trace) and MALDI-2 (red trace). Inset shows an enlarged mass region of m/z 120-200. (b) Comparison of the number of tissue-specific peaks detected using MALDI and MALDI-2 (error bars represent ± one standard deviation.(c-g) Selected ion images of tentatively identified arginine (m/z 173.1047), hexose (m/z 179.0565), phosphoglyceric acid (PGA) (m/z 184.9859), uridine (m/z 243.0621) and inosine (m/z 267.0735) with the accompanying MALDI and MALDI-2 derived signal traces. Images displayed were generated from the MALDI-2 dataset with TIC normalisation applied. Mass error is reported at <3 ppm for all metabolites. (h) Optical microscopy image of H&E stained mouse kidney performed after MSI. Tissue tears are a result of the dehydration process involved with staining.

To further evaluate the added metabolite coverage using MALDI-2 we utilised the METASPACE annotation platform[7] and compared MALDI-2 metabolite annotations obtained at 10% false discovery rate and detected in at least 2/3 technical replicates. Compared to MALDI datasets using NEDC matrix from 140 human and mouse kidney datasets, and only considering annotations found in ≥10% of these datasets, MALDI-2 resulted in 63 unique annotations (Figure 2). These results further highlight the added metabolite coverage achieved using MALDI-2.

METASPACE Annotations(≤ 10% FDR)

MALDI-2 (This Study) **Human** (MALDI + NEDC Matrix)

63 (≥ 2/3 datasets) **25** **204** (138 datasets)

5 **6** **1**
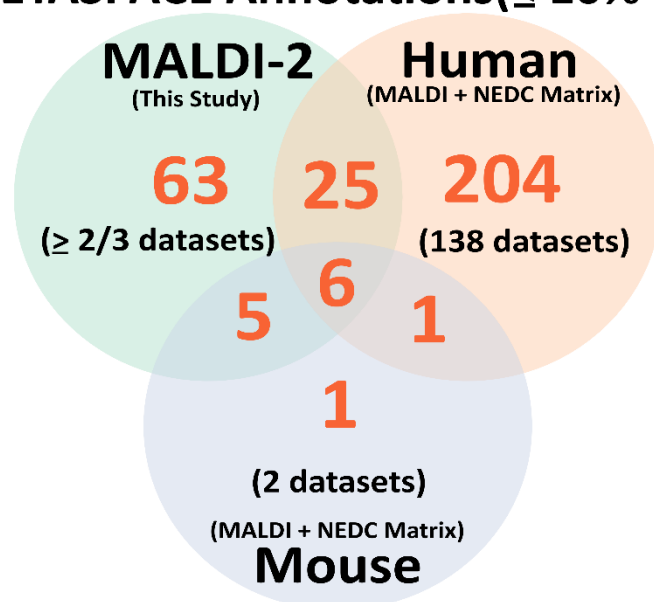
1

(2 datasets)

(MALDI + NEDC Matrix)

Mouse

Figure 2: METASPACE annotation results for n=3 of MALDI-2 kidney datasets compared to 140 public datasets. In all datasets, only on-tissue annotations at a false discovery rate (FDR) of 10% were considered. See ESI for details on data constraints.

In the field of cancer research, obtaining comprehensive spatial data across various metabolic pathways is imperative for identifying potential biomarkers and therapeutic targets, given the significant roles played by altered metabolism and metabolic reprogramming in cancer progression.[8] Thus we next applied MALDI-2-MSI to investigate a tumour bearing mouse liver tissue section. Fig.3a shows the H&E stained optical image with annotations of the tumour mass and surrounding normal liver tissue. Fig.1b shows that the *m/z* 146.0461 ion assigned as

[glutamate-H]⁻ and the *m/z* 259.0224 ion assigned as [glucose-6-phosphate-H]- are distributed specifically to the tumour and normal tissue regions respectively. The spectral profiles of the tumour site and normal tissue region (Fig.S4, ESI†) revealed significant changes in signal intensity for several ions. A spectral comparison of tumour and surrounding tissue, along with several selected ion images is provided in the ESI (Fig.S4 and S5, ESI†). Fig.3c displays the acquired average MALDI (black) and MALDI-2 (red) spectra acquired from adjacent sections. The base peak observed in the MALDI dataset was the [M-H]⁻ ion of glutathione (*m/z* 306.0765). Using MALDI-2 a significant increase in many low mass signals was observed (Fig.3c) with glutathione increasing 4-fold. Fig.3c inset shows additional ions found to significantly increase using MALDI-2, including the [M-H]⁻ ions of hexose (*m/z* 179.0565), uridine (*m/z* 243.0621), adenosine monophosphate (AMP) (*m/z* 346.0553) and linoleic acid (FA 18:2) (*m/z* 279.233).
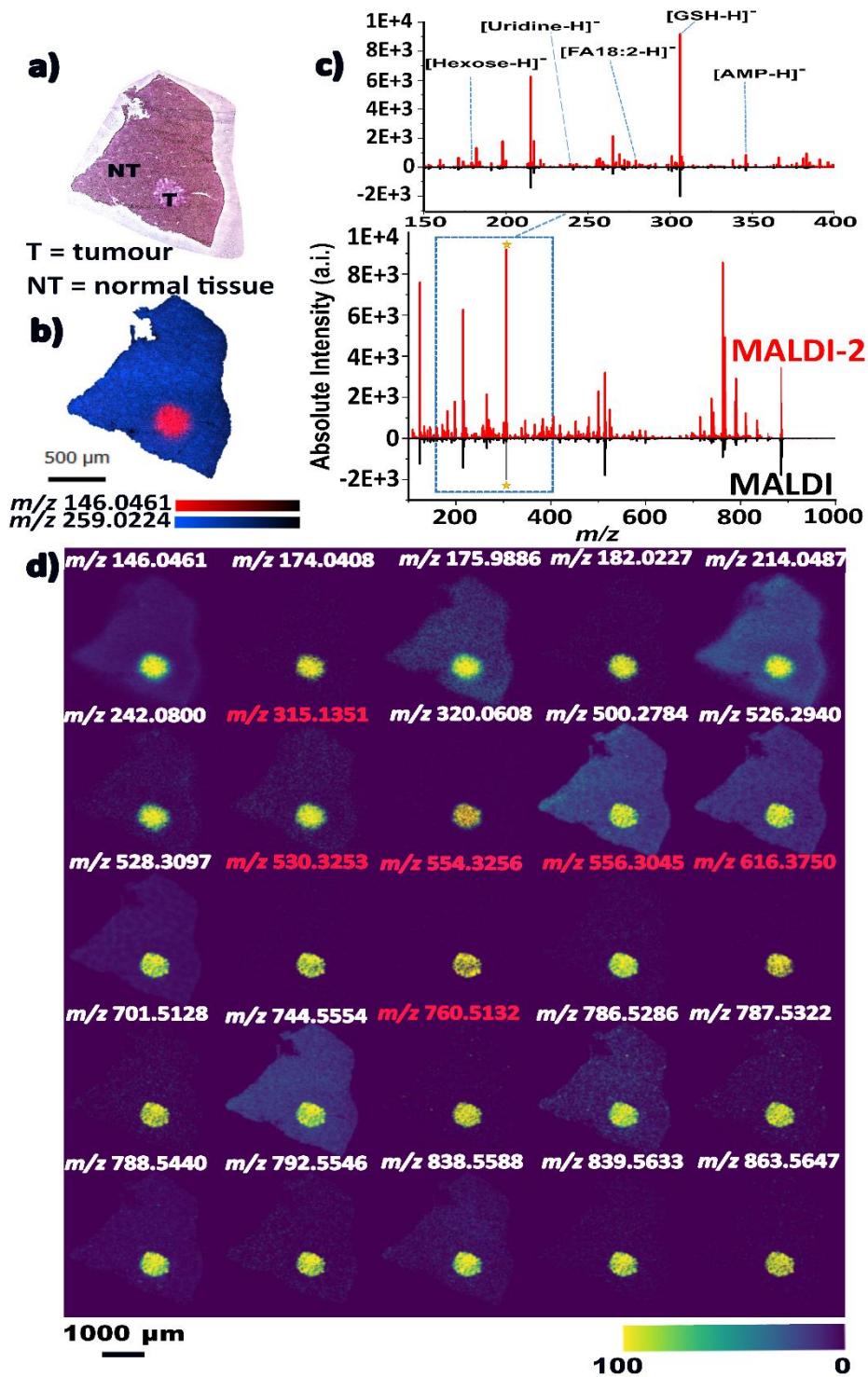
Figure 3: (a) optical image of the post-MSI Haemotoxylin and Eosin stained tissue section with the tumour bearing region (T) and normal surrounding liver tissue (NT) regions labelled. (b) Overlayed ion images for the[M-H]⁻ ions of glutamate (red) (m/z 145.0461, 1.3 ppm) and glucose-6-phosphate (blue) (m/z 259.0224, 0.1 ppm). (c) Averaged mass spectra acquired using (black trace) and MALDI-2 (red trace) derived datasets. Inset displays an enlarged m/z 150-400) region with tentatively identified metabolites [Hexose-H]⁻ (m/z 179.0565, 2.2 ppm), [Uridine-H]⁻ (m/z 243.0621, -0.4 ppm), linoleic acid [FA 18:2-H]⁻ (m/z 279.2330, 0.3 ppm), [Glutathione-H]⁻ (GSH) (m/z 306.0765, 0.1 ppm) and [Adenosine monophosphate-H]⁻ (AMP) (m/z 346.0553, -1.4 ppm). (d) MALDI-2 ion images with a Pearson correlation coefficient ≥0.6 for the tumour region marked (a) red values indicate ions only detected using MALDI-2.

To follow, we applied a co-localisation analysis to the tumour region visible via histology (Fig.3a) and extracted ions with a Pearson correlation coefficient for the tumour region ≥0.6. Fig.3d shows the colocalised ions and their corresponding distributions (ions not detected using MALDI are labelled in red). Fold change comparisons between MALDI and MALDI-2 are provided in the Table S1 (ESI†), revealing that all tumor-specific signals increase in signal intensity by up to 20-fold using MALDI-2. MALDI-2 improved the detection of metabolites such as small amino acids, including glutamate (*m/z* 146.0461) and *N*-acetyl-aspartic acid (*m/z* 174.0408), lipid precursors such as glycerophosphoethanolamine (*m/z* 214.0487), *N*-acylamides such as in the case of β-citrylglutamic acid (*m/z* 320.0608) and multiple lipid species. A full list of possible annotations for the species shown in Figure 3d is provided in the ESI.

Conclusion

This work has provided the first study investigating the advantages of MALDI-2 for the MSI of metabolites in tissue sections. Compared to conventional MALDI, MALDI-2 enabled the detection of a broader range of metabolites and increased overall sensitivity for many others that are also detected using MALDI. The advantages enable MSI to provide a deeper understanding of altered metabolism throughout heterogeneous tissues and will likely enable improvements in spatial resolution of metabolite MSI that leverage the gains in sensitivity. Given the increasing adoption of MALDI, including commercially available systems, it is anticipated these benefits stand to strengthen many metabolic studies using MSI.

Acknowledgement

References

1   A. Ly, A. Buck, B. Balluff, N. Sun, K. Gorzolka, A. Feuchtinger, K. P. Janssen, P. J. K. Kuppen, C. J. H. Van De Velde, G. Weirich, F. Erlmeier, R. Langer, M. Aubele, H. Zitzelsberger, L. McDonnell, M. Aichler and A. Walch, *Nat. Protoc. 2016 118*, 2016, 11, 1428–1443.

2   S. Schulz, M. Becker, M. R. Groseclose, S. Schadt and C. Hopf, *Curr. Opin. Biotechnol.*, 2019, 55, 51–59.

3   A. P. Bowman, R. M. A. Heeren and S. R. Ellis, *TrAC Trends Anal. Chem.*, 2019, 120, 115197.

4   R. R. Drake, T. W. Powers, E. E. Jones, E. Bruner, A. S. Mehta and P. M. Angel, *Adv. Cancer Res.*, 2017, 134, 85–116.

5   V. Llombart, S. A. Trejo, S. Bronsoms, A. Morancho, M. Feifei, J. Faura, T. García-Berrocoso, A. Simats, A. Rosell, F. Canals, M. Hernández-Guillamón and J. Montaner, *J. Proteomics*, 2017, 152, 243–253.

6   L. Rappez, M. Stadler, S. Triana, R. M. Gathungu, K. Ovchinnikova, P. Phapale, M. Heikenwalder and T. Alexandrov, *Nat. Methods 2021 187*, 2021, 18, 799–805.

7   T. Bien, K. Koerfer, J. Schwenzfeier, K. Dreisewerd and J. Soltwisch, *Proc. Natl. Acad. Sci. U. S. A.*, 2022, 119, e2114365119.

8   A. R. Buchberger, K. DeLaney, J. Johnson and L. Li, *Anal. Chem.*, 2018, 90, 240–265.

9   M. R. L. Paine, P. C. Kooijman, G. L. Fisher, R. M. A. Heeren, F. M. Fernández and S. R. Ellis, *J. Mater. Chem. B*, 2017, 5, 7444–7460.

10   Y. Fujimura and D. Miura, *Metabolites*, 2014, 4, 319–346.

11   D. Miura, Y. Fujimura, M. Yamato, F. Hyodo, H. Utsumi, H. Tachibana and H. Wariishi, *Anal. Chem.*, 2010, 82, 9789–9796.

12   T. J. A. Dekker, E. A. Jones, W. E. Corver, R. J. M. van Zeijl, A. M. Deelder, R. A. E. M. Tollenaar, W. E. Mesker, H. Morreau and L. A. McDonnell, *Anal. Bioanal. Chem.*, 2015, 407, 2167–2176.

13   E. Tanaka, Y. Ogawa, R. Fujii, T. Shimonaka, Y. Sato, T. Hamazaki, T. Nagamura-Inoue, H. Shintaku and M. Tsuji, *Sci. Reports 2020 101*, 2020, 10, 1–12.

14   R. J. Carreira, R. Shyti, B. Balluff, W. M. Abdelmoula, S. H. Van Heiningen, R. J. Van Zeijl, J. Dijkstra, M. D. Ferrari, E. A. Tolner, L. A. McDonnell and A. M. J. M. Van Den Maagdenberg, *J. Am. Soc. Mass Spectrom.*, 2015, 26, 853–861.

15   G. Wang, B. Heijs, S. Kostidis, A. Mahfouz, R. G. J. Rietjens, R. Bijkerk, A. Koudijs, L. A. K. van der Pluijm, C. W. van den Berg, S. J. Dumas, P. Carmeliet, M. Giera, B. M. van den Berg and T. J. Rabelink, *Nat. Metab. 2022 49*, 2022, 4, 1109–1118.

16   M. E. Dueñas, A. T. Klein, L. E. Alexander, M. D. Yandeau-Nelson, B. J. Nikolau and Y. J. Lee, *Plant J.*, 2017, 89, 825–838.

17   M. Dilillo, R. Ait-Belkacem, C. Esteve, D. Pellegrini, S. Nicolardi, M. Costa, E. Vannini, E. L. De Graaf, M. Caleo and L. A. McDonnell, *Sci. Reports 2017 71*, 2017, 7, 1–11.

18   M. Pietrowska, H. C. Diehl, G. Mrukwa, M. Kalinowska-Herok, M. Gawin, M. Chekan, J. Elm, G. Drazek, A. Krawczyk, D. Lange, H. E. Meyer, J. Polanska, C. Henkel and P. Widlak, *Biochim. Biophys. Acta - Proteins Proteomics*, 2017, 1865, 837–845.

19   F. Kanter, J. Lellmann, H. Thiele, S. Kalloger, D. F. Schaeffer, A. Wellmann and O. Klein, *Cancers (Basel),* 15, 3.

20   S. N. Jackson, L. Muller, A. Roux, B. Oktem, E. Moskovets, V. M. Doroshenko and A. S. Woods, *J. Am. Soc. Mass Spectrom.*, 2018, 29, 1463–1472.

21   C. D. Calvano, A. Monopoli, T. R. I. Cataldi and F. Palmisano, *Anal. Bioanal. Chem. 2018 41017*, 2018, 410, 4015–4038.

22   E. A. Elia, M. Niehaus, R. T. Steven, J.-C. Wolf and J. Bunch, 2020, 92, 23, 15285-15290

23   C. Bookmeyer, U. Röhling, K. Dreisewerd and J. Soltwisch, *Angew. Chemie Int. Ed.*, 2022, 61, e202202165.

24   J. Soltwisch, H. Kettling, S. Vens-Cappell, M. Wiegelmann, J. Müthing and K. Dreisewerd, *Science (80-.).*, 2015, 348, 211–215.

25   A. P. Bowman, J. F. J. Bogie, J. J. A. Hendriks, M. Haidar, M. Belov, R. M. A. Heeren and S. R. Ellis, *Anal. Bioanal. Chem.*, 2020, 412, 2277–2289.

26   T. Bien, E. A. Hambleton, K. Dreisewerd and J. Soltwisch, *Anal. Bioanal. Chem.*, 2021, 413, 2767–2777.

27   F. P. Y. Barré, M. R. L. Paine, B. Flinders, A. J. Trevitt, P. D. Kelly, R. Ait-Belkacem, J. P. Garcia, L. B. Creemers, J. Stauber, R. J. Vreeken, B. Cillero-Pastor, S. R. Ellis and R. M. A. Heeren, *Anal. Chem.*, 2019, 91, 10840–10848.

28   B. Heijs, A. Potthoff, J. Soltwisch and K. Dreisewerd, *Anal. Chem.*, 2020, 92, 13904–13911.

29   J. C. McMillen, D. B. Gutierrez, A. M. Judd, J. M. Spraggins and R. M. Caprioli, *J. Am. Soc. Mass Spectrom.*, 2021, 32, 2583–2591.

30   A. P. Bowman, J. F. J. Bogie, J. J. A. Hendriks, M. Haidar, M. Belov, R. M. A. Heeren and S. R. Ellis, *Anal. Bioanal. Chem.*, 2020, 412, 2277.

31   M. Niehaus, J. Soltwisch, M. E. Belov and K. Dreisewerd, *Nat. Methods 2019 169*, 2019, 16, 925–931.

32   T. Sarretto, X. Spotbeen, T. Gevaert, S. Joniau, J. V Swinnen, A. J. Trevitt, S. R. Ellis, A. J. Trevitt, S. R. Ellis and S. Joniau, *Anal. Sens.*, 2022, 2, e202100052.

33   C. Damiana Calvano, T. R. I Cataldi, J. F. Kögel, A. Monopoli, F. Palmisano and J. Sundermeyer, *J. Am. Soc. Mass Spectrom*, 2017, 28, 1666–1675.

34   A. Palmer, P. Phapale, I. Chernyavsky, R. Lavigne, D. Fay, A. Tarasov, V. Kovalev, J. Fuchser, S. Nikolenko, C. Pineau, M. Becker and T. Alexandrov, *Nat. Methods 2016 141*, 2016, 14, 57–60.

35   D. Hanahan and R. A. Weinberg, *Cell*, 2011, 144, 646–674.